Nanocomposite Zn_2SnO_4/SnO_2 Thick Films as a Humidity Sensing Material

Maria Vesna Nikolic, *Senior Member, IEEE* , Milena P. Dojcinovic, Zorka Z. Vasiljevic, Miloljub D. Lukovic and Nebojsa J. Labus

***Abstract*— Nanocomposite Zn_2SnO_4/SnO_2 powder was obtained by solid state synthesis from homogenized starting nanopowders of ZnO and SnO_2, mixed in the 1:1 molar ratio, structurally and morphologically characterized using X-ray diffraction (XRD) and Scanning Electron Microscopy (SEM). Thick film paste was made by adding organic vehicles to the obtained powder. Three to five layers (layer thickness approx. 12 μm) were screen printed on alumina substrate with small test PdAg electrodes and fired at 600ºC for 30 minutes. SEM analysis confirmed formation of a porous structure suitable for humidity sensing. Impedance response was studied at the working temperatures of 25 and 50ºC in a humidity chamber where the relative humidity (RH) was 30-90% and measured frequency 42 Hz – 1 MHz. With increase in film thickness the overall sensor impedance increased. It reduced at 100 Hz from 36 to 0.25 MΩ (60 μm), from 23.4 to 0.25 MΩ (48 μm) and from 6.8 to 0.02 MΩ (36 μm) at 25 ºC, while at 50 ºC and also 100 Hz it reduced from 14 MΩ to 0.72 MΩ (48 μm) for RH 30 and 90%, respectively. The response (8 s) and recovery (10 s) was fast, showing that this nanocomposite has potential for application in humidity sensing.**

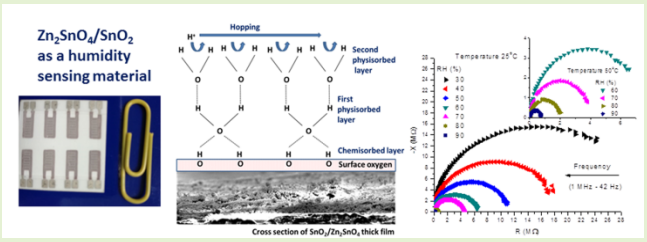

***Index Terms*— Thick film sensors, nanostructured materials, impedance measurement**

I. Introduction

Metal oxide based materials have been widely investigated as gas sensing materials, as they are robust, highly sensitive, exhibit a fast response time and are inexpensive [1]. Humidity monitoring and humidity sensors are essential components of future sensor nodes. They are part of the first tier in future Internet of Things (IoT) networking platforms [2]. Humidity sensors are also widely applied in determining the soil water content [3]. Many different metal oxides have been investigated for gas and humidity sensing. One path for improvement of gas sensing materials is to combine metal oxides together in order to achieve improved properties [4-8]. Better hysteresis and faster response have been achieved using composite sensors [4]. Use of metal oxide nanostructures in gas and vapour sensing has led to improved thermal and chemical stability, sensitivity and selectivity performance [9].

An earlier version of this paper was presented at the 2019 IEEE International Conference on Flexible and Printable Sensors and Systems (FLEPS) and was published in its Proceedings https://ieeexplore.ieee.org/document/8792304.

This work was supported by the Ministry for Education, Science and Technological Development of the Republic of Serbia, projects III45007 and III45014.

M. V. Nikolic, M. P. Dojcinovic and M. D. Lukovic are with the Institute for Multidisciplinary Research, University of Belgrade, 11030 Belgrade, Serbia (e-mail: mariav@rcub.bg.ac.rs; milena.dojcinovic@imsi.rs; lukovic@imsi.rs).

Z. Z. Vasiljevic and N. J. Labus are with the Institute of Technical Sciences of SASA, 11000 Belgrade, Serbia (e-mail: zorka.djuric@itn.sanu.ac.rs; nebojsa.labus@itn.sanu.ac.rs).

Tin-based functional semiconductors such as SnO_2 and Zn_2SnO_4 have been the subject of much research due to promising application in solar cells, photocatalysis, gas sensors and lithium ion batteries [10-16]. Zinc oxide (ZnO) and tin oxide (SnO_2) have been extensively investigated as gas sensors [6, 17, 18]. Tin oxide (SnO_2) is a metal oxide n-type semiconductor with a direct band gap of about 3.6 eV , with a large number of defect sites in the form of oxygen vacancies and Sn interstitials responsible for adsorption and desorption of water molecules [4]. One of the main drawbacks of SnO_2 humidity sensors are long response, slow recovery times and low hysteresis, but good sensitivity [4, 19]. Improved hysteresis and faster response/recovery times have been obtained using composite ZnO-SnO_2 sensors [4].

Zinc-stannate (Zn_2SnO_4) can be obtained by solid-state synthesis of ZnO and SnO_2. It is a cubic spinel oxide n-type semiconductor with a direct band gap in the range 3.35-4.1 eV [20], high electron mobility and conductivity [21, 22]. Zinc-stannate has shown high selectivity and sensitivity to both oxidizing and reducing gases, so has been studied as a NO, NO_2, C_2H_5OH sensing material [23, 24], but not widely as a humidity sensing material [21]. Stambolova *et al* [25] studied humidity sensing properties of spinel stannate thin films, while Kovacheva *et al* [26] determined that pure Zn_2SnO_4 had lower sensitivity and significantly lower conductivity than Mg substituted Zn_2SnO_4, with Mg_2SnO_4 showing the highest relative humidity sensitivity.

Much work has focused on Zn_2SnO_4/SnO_2 composites for application in gas sensing. As these two materials have

different work functions, n-n heterojunctions can form at their interface. The conduction band edge of Zn_2SnO_4 is located at a higher potential than SnO_2 leading to electron transfer until Fermi level alignment. This results in formation of additional electron depletion layers at the heterojunction interface, causing a larger resistance decrease when exposed to gases or humidity [27, 28]. Recently Sun et al [10] achieved improved formaldehyde sensing performance of this composite by synthesizing hollow microspheres. Moon *et al* [5] determined that adding small amounts of spinel Zn_2SnO_4 to SnO_2 improved sensitivity to CO gas in the temperature range 150-300ºC, while Yu and Choi [22] investigated variations of $ZnO/SnO_2/Zn_2SnO_4$ layered sensors. Investigation of the sensitivity of porous Zn_2SnO_4/SnO_2 hierarchical spheres to triethylamine [27] and Zn_2SnO_4-doped SnO_2 hollow spheres to phenylamine [28] confirmed that composites of these two metal oxides express improved gas sensing properties.

Commercial metal oxide sensors are commonly obtained by screen-printing paste on a sensor substrate with electrodes. Alumina (ceramic material) has been most often used as the sensor substrate [10,17,18,22], though glass has been used too [4]. Much recent research has focused on using diverse flexible sensor substrates enabling much more versatile and different sensor applications and opening the door to wearable electronics [29-32]. Interdigitated Ag, Ag-Pd or Au electrodes are most often printed on the substrate by screen-printing [4, 14] or inkjet printing techniques [30].

In this work we have focused on the sensing material. To the best of our knowledge we have found no literature data on humidity sensing properties of composite Zn_2SnO_4/SnO_2, even though it has shown improved gas sensing properties to different gases as described above. Thus, Zn_2SnO_4/SnO_2 composite nanocrystalline powder was obtained by solid state synthesis, a simple and industrially applicable technique used for obtaining powders [33]. Possible application of nanocomposite Zn_2SnO_4/SnO_2 thick films screen printed on alumina substrate with test PdAg interdigitated electrodes in humidity sensing was analysed by monitoring the change in impedance with humidity.

II. Materials and Methods

A. Synthesis and characterization of Zn_2SnO_4/SnO_2 nanocrystalline powder

A homogenized mixture (molar ratio 1:1) of zinc-oxide (ZnO, Sigma Aldrich, particle size <100 nm) and tin oxide (SnO_2, Sigma Aldrich, particle size < 100 nm) nanopowders was calcined at 1050 ºC for 2 hours in air in order to obtain Zn_2SnO_4/SnO_2 nanocrystalline composite powder. X-ray diffraction patterns of the powder were recorded on a Rigaku RINT2000 diffractometer in the range 10-80º, with CuK_α (λ = 1.54178 Å) radiation. Powder morphology was analyzed by scanning electron microscopy (SEM) on a TESCAN Electron Microscope VEGA TS 5130 MM device. The average particle size was determined from SEM images taking into account at least 150 particles using the Semaphore software.

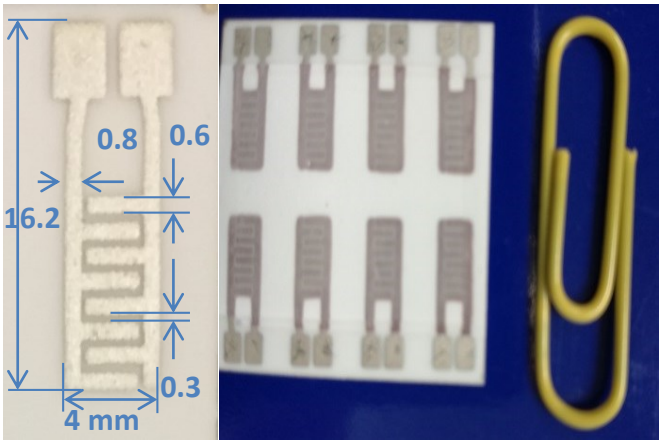

Fig. 1. Zn_2SnO_4/SnO_2 nanocomposite thick film samples printed on alumina substrate with test PdAg electrodes (right) and PdAg electrode with dimensions given in mm (left)

B. Thick film preparation and characterization

Thick film paste was made by mixing the obtained Zn_2SnO_4/SnO_2 powder with organic vehicles using the procedure of Ito et al [34] we have previously applied for other mixed metal oxide thick film samples [35].

Small interdigitated PdAg electrodes with an outer dimension 16.2 x 4 mm, finger width 0.6 mm, finger spacing 0.3 mm (shown in detail on Fig. 1) were screen printed on alumina substrate and fired at 850ºC in a conveyer furnace. Then, 3-5 layers of thick film paste (the average layer thickness was 12 µm) were screen printed on the prepared substrate with electrodes. Each layer was dried for 20 min at 100ºC before the next layer was printed. Finally, thick film samples were fired at 600ºC for 30 minutes in air in a chamber furnace. An example is shown in Fig. 1. SEM images of the sample surface and cross-section were recorded on the same device as described above.

C. Complex impedance measurements

Change in complex impedance of Zn_2SnO_4/SnO_2 thick film samples was monitored in a JEIO TECH TH-KE 025 temperature and humidity climatic chamber at working temperatures of 25 and 50 ºC in the frequency range 42 Hz to 1 MHz on a HIOKI 3532-50 LCR HiTESTER at a constant voltage of 5 V. The relative humidity (RH) was varied between 30 and 90 % in steps of 10 %. We also measured the bare intedigital PdAg structure on the alumina substrate at the working temperature of 25ºC under the same conditions as Zn_2SnO_4/SnO_2 thick film samples.

III. Results and Discussion

A. Structure and morphology of Zn_2SnO_4/SnO_2 nanocrystalline powder and thick film samples

XRD analysis of the obtained powder confirmed the formation of cubic spinel Zn_2SnO_4 (space group $Fd\bar{3}m$, JCPDS 24-1470) as the first phase and remaining SnO_2 (tetragonal space group $P4_2/mnm$, JCPDS 88-0287) as the second phase in the Zn_2SnO_4/SnO_2 nanocrystalline powder (Fig. 2).

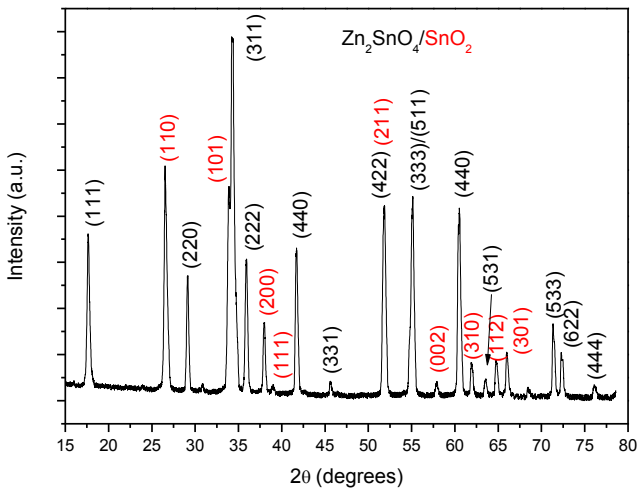

Fig. 2. XRD pattern Zn_2SnO_4/SnO_2 nanocomposite powder

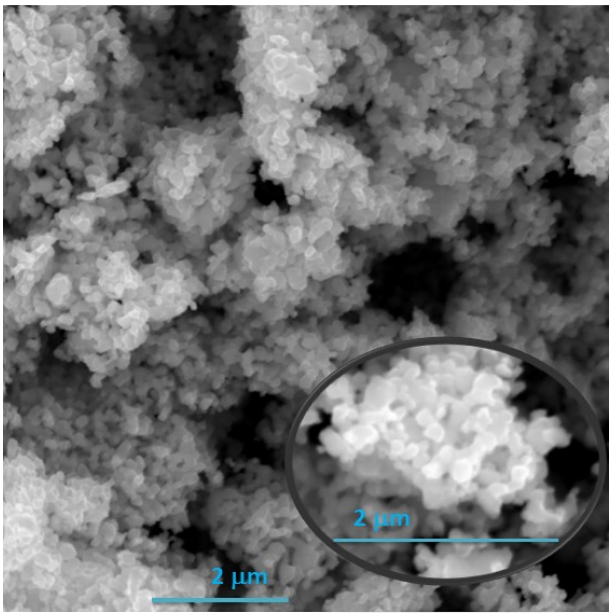

Fig. 3. SEM micrograph of Zn_2SnO_4/SnO_2 nanocomposite powder

No peaks for ZnO (JCPDS 77-0191) were observed as all ZnO reacted with SnO_2 to form Zn_2SnO_4 at the calcination temperature of 1050°C. Ma *et al* also noted pure phase Zn_2SnO_4 in the temperature interval 1000-1200 °C [36]. The average crystallite size for both phases was estimated using the Sherrer equation: $D = K\lambda/\beta\cos\theta$, where D is the crystallite size, K = 0.9 is the shape factor, λ is 1.54178 Å for Cu radiation and β is the full-width at half maximum. It was 58 nm for SnO_2 and 60 nm for Zn_2SnO_4.

The Zn_2SnO_4/SnO_2 powder was composed of relatively uniform nanoparticles forming aggregates (Fig. 3). The average particle size was estimated as 154 nm using an average of over 150 particles marked on several SEM micrographs and the Semaphore software.

This morphology did not change much for thick film samples. A SEM image of a Zn_2SnO_4/SnO_2 thick film sample surface is shown in Fig. 4a where we can see aggregates consisting of several smaller particles. The average particle size was determined as 155 nm using an average for over 200 particles, with the particle size distribution shown in Fig. 4b.

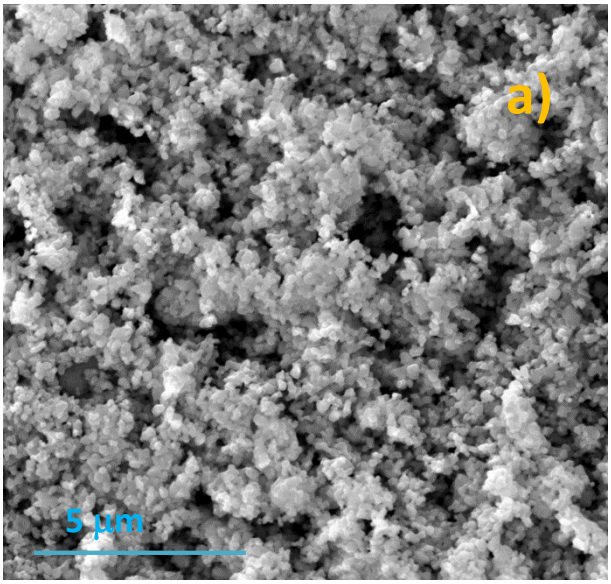

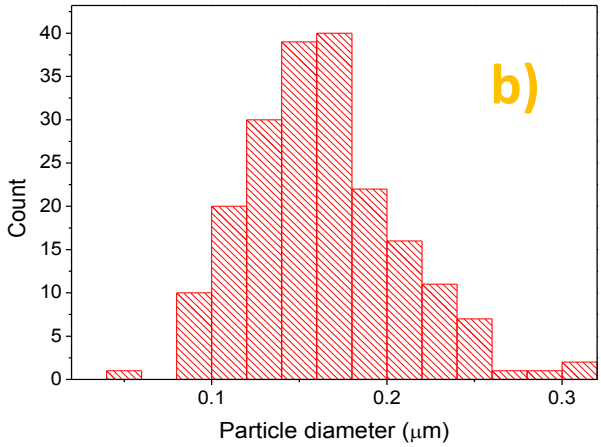

Fig. 4. SEM micrograph of Zn_2SnO_4/SnO_2 nanocomposite thick film sample surface - a) and particle size distribution - b)

B. Influence of change in relative humidity on impedance

The modulus of complex impedance decreased with frequency and also with increase in relative humidity for all analyzed samples, as shown on the example in Fig. 5. This was most expressed at lower frequencies, as shown in Fig. 6 at 100 Hz for two different sample thicknesses.

With increase in film thickness the overall sensor impedance increased. We have noted similar behavior for Fe_2TiO_5 thick film samples [35], where we analyzed samples with 3-5 thick film layers.

The measured impedance at 100 Hz (where the change in impedance is larger than at higher frequencies) at the working temperature of 25°C reduced from 36 to 0.25 MΩ (60 μm – five layers of screen printed thick film paste), from 23.4 to 0.25 MΩ (48 μm – four layers) and from 6.8 to 0.02 MΩ (36 μm – three layers) for relative humidity (RH) of 30 and 90%, respectively.

The microstructure of oxide ceramic materials is composed of grains, grain boundaries, surfaces and pores [37]. This makes them suitable for gas and humidity sensing as they

react with gas molecules. Thick film technology produces porous films with microstructural properties similar to bulk sintered samples, but on a smaller scale. Lopes at al [38] concluded that the impedance of thick film samples increased due to higher electron transport resistances in the bulk of the material with increase in film thickness. Saif and Poopalan [39] noted the opposite for $Ba_{0.6}Sr_{0.4}TiO_3$ thin films. In this case the impedance and permittivity decreased with the increase in film thickness. They attributed this phenomenon to reduction in grain size with decrease in thin film thickness. This was not the case in this work, where the sample microstructure did not change with increase in film thickness. The particle size did not change when we compare the powder (Fig. 3, 154 nm) and thick film sample surface (Fig. 4, 155 nm) due to the low firing temperature of thick film samples that enabled burn-out of the organics in the thick film paste, but did not induce grain growth.

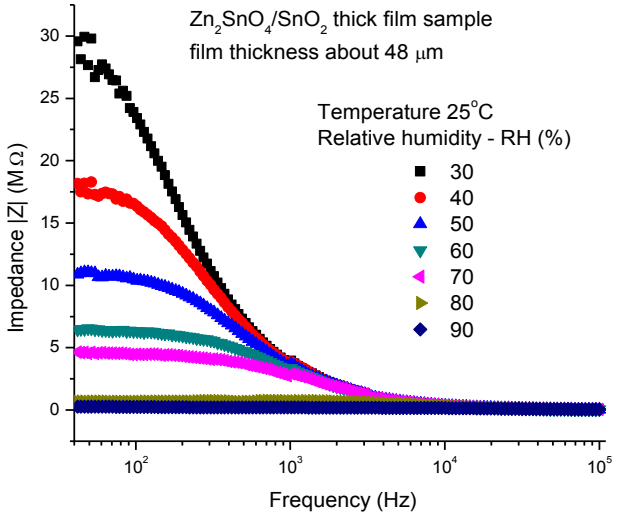

Fig. 5. Change of impedance of Zn_2SnO_4/SnO_2 nanocomposite thick film sample with frequency in the RH range 30 - 90% at the working temperature of 25 °C

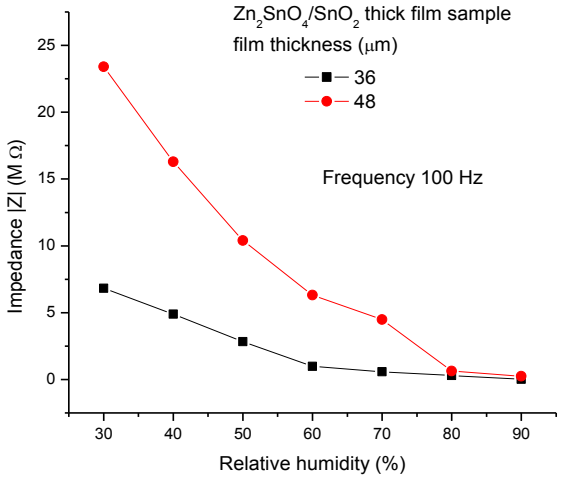

Fig. 6. Change of impedance of Zn_2SnO_4/SnO_2 nanocomposite thick film sample with RH at 100 Hz for different film thicknesses at the working temperature of 25 °C

At the higher working temperature of 50 °C the measured impedance of thick film samples changed in a similar way. Thus, for a 48 μm Zn_2SnO_4/SnO_2 thick film sample, at 100 Hz the measured impedance reduced from 14 to 0.72 MΩ, for RH of 30 and 90%, respectively.

The measured modulus of complex impedance of a reference sample with the bare interdigitated PdAg electrode structure was higher than the measured values for the sensing nanocomposite layer and also decreased with increase in frequency, but the change of impedance with increase in relative humidity was very small, as can be seen in Fig. 7 where the curves almost overlap. Thus, at 100 Hz, as shown in the inset in Fig. 7, the impedance reduced from 62.74 to 57.74 MΩ, for RH of 30 and 90%, respectively. This is a very small change in impedance with increase in RH and was more expressed for RH 70-90%, compared to the change in impedance with increase in RH of the Zn_2SnO_4/SnO_2 nanocomposite thick film layer.

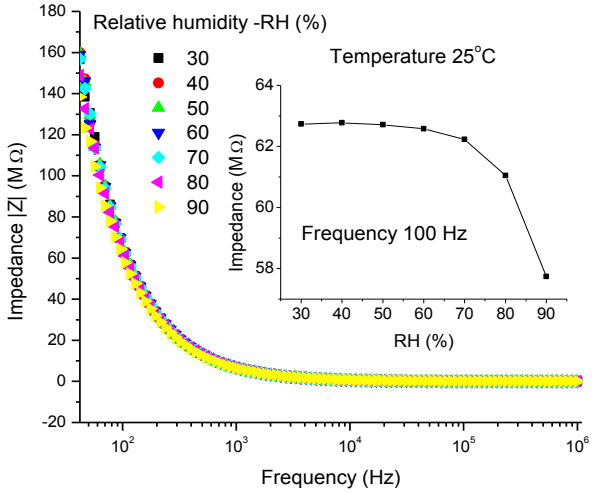

Fig. 7. Change of impedance of a reference sample of a bare PdAg interdigitated electrode structure printed on alumina substrate (as shown in Fig. 1) with frequency in the RH range 30 - 90% at the working temperature of 25 °C; inset: Impedance reduction with RH at 100 Hz

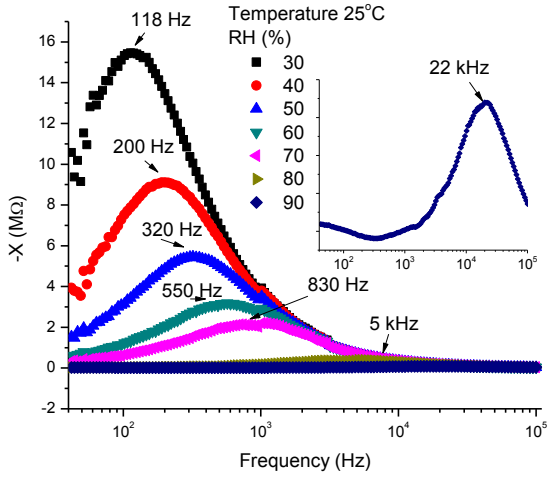

Fig. 8. Change of imaginary part of impedance (-X) for a Zn_2SnO_4/SnO_2 nanocomposite thick film sample with frequency in the RH range 30-90% at the working temperature of 25 °C; inset: change of -X with frequency for RH 90 %

The dependence of the imaginary part of impedance (-X) on frequency is shown in Fig. 8. Relaxation peaks noted in these curves are due to space charge relaxation [40]. Shift of the relaxation peak to higher frequencies is noticeable with increase in relative humidity (RH), especially for RH 80 % and 90%, besides a decrease of -X with increase in RH. Shift of the relaxation peak to higher frequencies with increase in RH has been previously noted for other ceramic oxide materials [41].

The sensitivity was calculated as $S = \Delta Z/\Delta RH$ and represents the ratio between the change of sensor impedance and RH% [4]. It depended on the thick film thickness and working temperature. It was calculated as 0.68±0.110, 0.38±0.0463 and 0.11±0.019 MΩ/%RH for the working temperature of 25°C and film thickness of about 60, 48 and 36 µm, respectively. The sensitivity increased with the film thickness, but the error did also, so we would select the film thickness of about 48 µm as optimal for this sensing material electrode configuration. The determined sensitivity was lower for the higher working temperature of 50°C, with 0.25±0.029 MΩ/%RH determined for the 48 µm thick film, showing that the working temperature also had an influence on sensitivity.

A complex impedance (R + jX) plot obtained for of a Zn_2SnO_4/SnO_2 thick film sample (film thickness about 48 µm) is shown in Fig. 9, measured at the working temperature of 25°C in the RH range 30 - 90 % and at the working temperature of 50°C in the RH range 60 – 90 % (inset). With increase in RH the complex impedance semicircular arc shrank and started resembling a semicircle. The existence of only one semicircle/semicircular arc reflected the dominant influence of the grain boundary component [35, 40-43]. The impedance data is usually modeled with an equivalent circuit containing bulk and grain boundary components (consisting of a parallel resistance/capacitance) [42, 43]. Depending on the analyzed ceramic oxide material there are either two semicircular arcs (low frequency side due to the grain boundary conduction and high frequency side due to the bulk/grain conduction) or one where the influence of these two components overlap, or one component (usually the grain boundary conduction) is dominant [40, 42]. Variation in the conduction between grains results in change in the grain boundary resistance and grain boundaries represent active sites for the dissociation of gas/water molecules [4]. The relaxation frequency represents the maximum frequency of a complex impedance semicircle, and its reciprocal value is defined as the relaxation time [40]. It usually shifts to higher values with increase in sample temperature [42] and we have previously noted shift of the relaxation frequency to higher values with increase in RH for other ceramic oxide materials [35, 41].

The measured complex impedance data was analyzed using an equivalent circuit consisting of a parallel resistance and capacitance element (shown as an inset in Fig. 10) and the EIS Spectrum Analyzer Software [44]. For a Zn_2SnO_4/SnO_2 thick film sample (film thickness 48 µm) the determined equivalent (grain boundary) resistance and relaxation frequency at the working temperature of 25 °C is shown in Fig. 10.

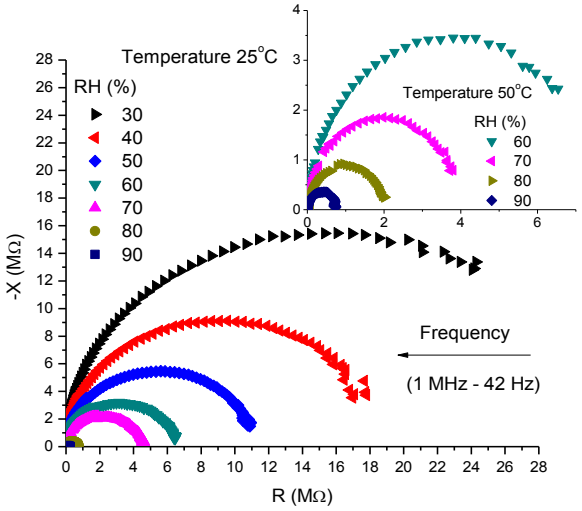

Fig. 9. Complex impedance (R + jX) plot for a Zn_2SnO_4/SnO_2 nanocomposite thick film sample (film thickness about 48 µm) in the RH range 30-90% at the working temperature of 25 °C and frequency range 42- Hz- 1 MHz; inset: complex impedance plot for same sample in the RH range 60-90 % at the working temperature of 50°C and frequency 42 Hz – 1 MHz

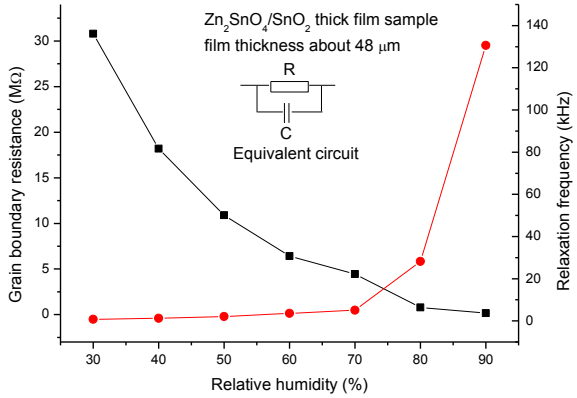

Fig. 10. Grain boundary resistance and relaxation frequency determined for a Zn_2SnO_4/SnO_2 thick film sample (film thickness about 48 µm) in the RH range 30-90% at the working temperature of 25 °C; inset: equivalent circuit

The relaxation frequency increased slowly with increase in RH from 0.75 kHz (RH 30%) to 5 kHz (RH 70%) and then more rapidly for high RH values of 80 and 90%. The grain boundary capacitance increased slightly with increase in RH from 43.07 pF (RH 30%) to 45.02 pF (RH 90%). The grain boundary resistance decreased with increase in RH in accordance with the humidity sensing mechanism. Grain boundaries represent active sites for the dissociation of water molecules, so increase in RH leads to adsorption of water molecules [4]. The humidity sensing mechanism consists of two processes: chemisorption and physisorption and they depend on the RH value [4, 35]. At low RH water molecules are chemisorbed on the thick film surface forming a chemisorbed hydroxide layer that requires significant energy for hopping transfer and the impedance is high, as shown in Fig. 11.

As RH increases, a physisorption of water molecules takes place over the chemisorbed layer. Single hydrogen bonding enables mobility of water molecules. Less energy is required.

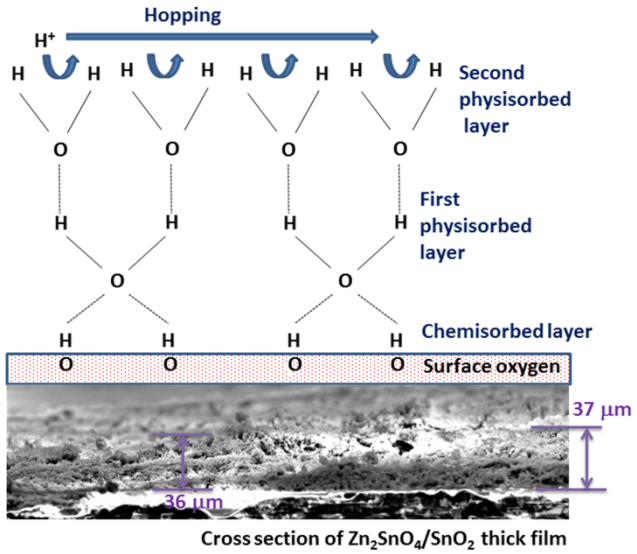

Fig. 11. Schematic illustration of the humidity sensing mechanism

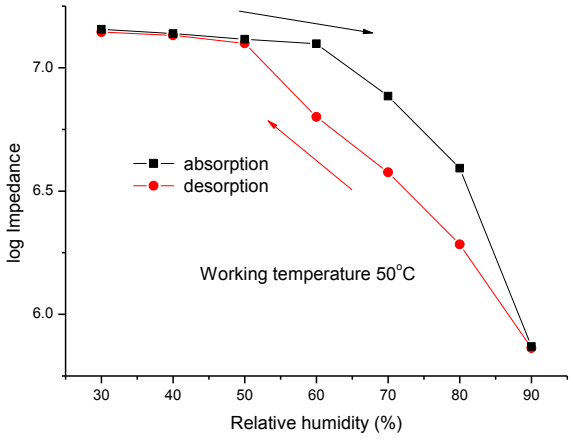

Fig. 12. Absorption and desorption (hysteresis) curves obtained for a Zn_2SnO_4/SnO_2 thick film sample (film thickness about 48 µm) in the RH range 30-90% at the working temperature of 50 °C

Further increase in RH leads to the formation of multilayers of physisorbed water, where the water molecule and proton combine forming a H_3O^+ species that releases a proton to a neighboring water molecule, initiating a chain reaction, known as the Grotthuss chain reaction. Ionic conductivity increases and impedance decreases.

The hysteresis needs to be low for a good sensing material. It represents the time delay between absorption and desorption processes. At the frequency of 100 Hz we obtained an overall value below 15%, for analysis of different film thickness values (36-60 µm) and at both working temperatures (25 and 50 °C). An example is given in Fig. 12 for a Zn_2SnO_4/SnO_2 sample (film thickness 48 µm, working temperature 50 °C) where the hysteresis value was 13.5%. This value is slightly high and this parameter needs to be improved. This can be achieved by improving the sensing material microstructure by reducing grain size that can be achieved with different synthesis process, or by changing its composition.

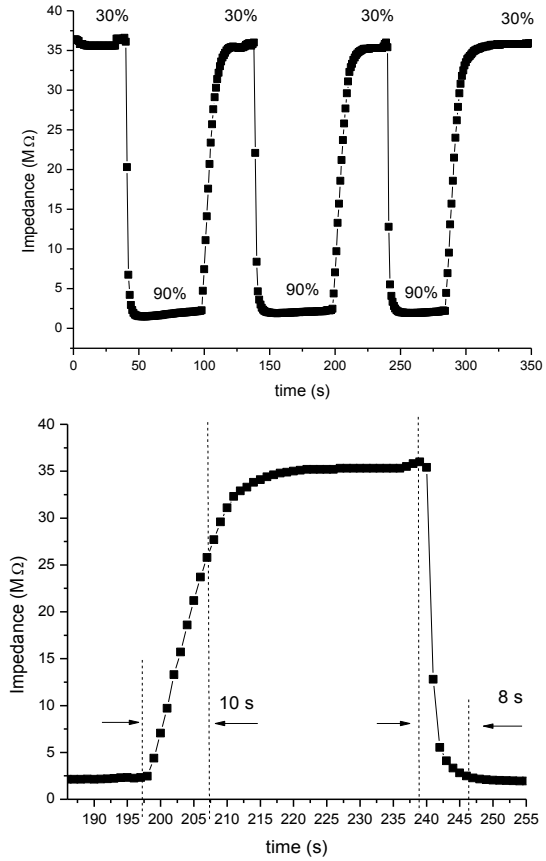

Fig. 13. Response and recovery times obtained for a Zn_2SnO_4/SnO_2 thick film sample (film thickness about 60 µm) in the RH range 30-90% at the working temperature of 25 °C

The time the sensor needs to reach 90% of the total response when exposed to a certain humidity level represents the response time, while the time it needs to return to 90% of the baseline signal represents the recovery time. We measured this at 100 Hz with the thick film sensor at room temperature and ambient humidity (estimated at 30%) and exposed it to RH of 90% in the humidity chamber, as shown in Fig. 13. The response time was about 10 s, while the recovery time was about 8 s. No noticeable drift was noted.

IV. Conclusion

We have analyzed possible application of Zn_2SnO_4/SnO_2 nanocomposite thick films screen printed on test interdigitated electrodes as a humidity sensing material and it shows promise as the impedance changed noticeably with change in RH in the range 30 – 90%, with sensitivity of 0.38±0.0463 MΩ/%RH at the working temperature of 25°C. Fast response and recovery was obtained, while the hysteresis needs to be improved. Further work will focus on analyzing how different synthesis methods change the microstructure. Sensitivity and selectivity towards other gases will also be analyzed. Another step is to go flexible and implement this sensing material on flexible electrodes.

REFERENCES

[1] G. F. Fine, L. M. Cavanagh, A. Afonja, R. Binions, "Metal oxide semi-conductor gas sensors in environmental monitoring", *Sensors*, vol. 10, pp. 5469-5502, 2010.

[2] M. S. Khan, M. S. Islam, H. Deng, "Design of a reconfigurable RFID sensing tag as a generic sensing platform toward the future Internet of Things", *IEEE Internet of Things Journal*, vol. 1, no. 4, pp. 300-310, 2014.

[3] J.-M. Tulliani, C. Baroni, L. Zavattaro, C. Grignani, "Strontium doped hematite as a possible humidity sensing material for soil water content determination", *Sensors*, vol. 13, pp. 12070-12092, 2013.

[4] M. Velumani, S. R. Meher, Z. C. Alex, "Impedometric humidity sensing characteristics of SnO_2 thin films and SnO_2-ZnO composite thick films grown by magnetron sputtering", *J. Mater. Sci.:Mater. Electron*., vol. 29, pp. 3999-4010, 2018.

[5] W. J. Moon, J. H. Yu, G. M. Choi, "Selective CO gas detection of SnO_2-Zn_2SnO_4 composite gas sensor", *Sens. Actuators B*, vol. 80, pp. 21-27, 2001.

[6] N. D. Md Sin, S. Ahmad, M. F. Malek, M. H. Mamat, M. Rusop, "Improvement sensitivity humidity sensor based on ZnO/SnO_2 cubic structure, *IOP Conf. Ser.:Mater. Sci. Eng*., vol. 46, 012005, 2013

[7] W. -P. Tai, J.-H. Oh, "Fabrication and humidity sensing properties of nanostructured TiO_2-SnO_2 thin films", *Sens. Actuators B*, vol. 85, pp. 154-157, 2002.

[8] S. S. Zhang, G. Sun, Y. Li, B. Zhang, L. Lin, Y. Wang, J. Cao, Z. Zhang, "Continuously improved gas-sensing performance of SnO_2/Zn_2SnO_4 porous cubes by structure evolution and further NiO decoration", *Sens. Actuators B.:Chem.*, vol. 255, pp. 2936-2943, 2018.

[9] P. Bindra, A. Hazra, "Capacitive gas and vapor sensors using nanomaterials", *J. Mater. Sci. Mater. Electron.*, vol. 29, pp. 6129-6148, 2018.

[10] G. Sun, G. Ma, Y. Li, Z. Zhang, Z. Chen, Y. Wang, J. Cao, H. Bala, "Improved formaldehyde-sensing performance of SnO_2/Zn_2SnO_4 nanocomposites by structural evolution", *Mater. Lett.*, vol. 191, pp. 145-149, 2017.

[11] D. An, N. Mao, G. Deng, Y. Zou, Y. Li, T. Wei, X. Lian, "Ethanol gas-sensing of the Zn_2SnO_4 nanospheres", *Ceram. Int.* vol. 42, pp. 3535-3541, 2016.

[12] S.-H. Choi, I.-S. Hwang, J.-H. Lee, S.-G. Oh, I.-D. Kim, 'Microstructural control and selective C_2H_5OH sensing properties of Zn_2SnO_4 nanofibers prepared by electrospinning", *Chem. Commun*., vol. 47, pp. 9315-9317, 2011.

[13] P. Junploy, A. Phuruangrat, N. Plubphon, S. Thongtem, T. Thongtem, "Photocatalytic degradation of methylene blue by Zn_2SnO_4-SnO_2 system under UV visible radiation", *Mater. Sci. Semicond. Proc.*, vol. 66, pp. 56-61, 2017.

[14] L. Sun, S. Li, Y. Su, D. He, Z. Zhang, 'Surface-disorder engineered Zn_2SnO_4/SnO_2 hollow microboxes with enhanced solar-driven photocatalytic activity", *Appl. Surface Sci.,* vol. 463, pp. 20534-20560, 2017.

[15] S. Sun, S. Liang, "Morphological zinc-stannate: synthesis, fundamental properties and applications", *J. Mater. Chem. A*, vol. 5, pp. 20534-20560, 2017.

[16] M. Masjedi-Arani, M. Salavati-Niasari, "Facile precipitation synthesis and electrochemical evaluation of Zn_2SnO_4 nanostructure as a hydrogen storage material", *Int. J. Hydrogen Energ.,* vol. 41, pp. 12420-12429, 2017.

[17] M. A Ponce, P. R. Bueno, J. Varela, M. S. Castro, C. M. Aldao, "Impedance spectroscopy analysis of SnO_2 thick-films gas sensors", *J. Mater. Sci.: Mater. Electron.*, vol. 19, pp. 1169-1175, 2008.

[18] Q. Qi, T. Zhang, Q. Yu, R. Wang, Y. Zheng, L. Liu, H. Yang, "Properties of humidity sensing ZnO nanorods-base sensor fabricated by screen-printing", *Sens. Actuators B: Chem*., vol. 133, pp. 638-643, 2008.

[19] Q. Kuang, C.Lao, L. W. Zhong, Z. Xie, L. Zheng, "High sensitivity humidity sensor based on a single SnO_2 nanowire", *J. Am. Chem.Soc.,* vol. 129, pp. 6070-6071, 2007.

[20] M. A. Apulche Aviles, Y. Wu, "Photoelectrochemical study of the band structure of Zn_2SnO_4 prepared by the hydrothermal method", *J. Am. Chem. Soc.*, vol. 131, pp. 3216-3224, 2009

[21] G. Fu, H. Chen, Z. Chen, J. Zhang, H. Kohler, "Humidity sensitive characteristics of Zn_2SnO_4-$LiZnVO_4$ thick films prepared by the sol-gel method", *Sens. Actuators B*, vol. 81, pp. 308-312, 2002

[22] J. H. Yu, G. M. Choi, "Current-voltage characteristics and selective CO detection of Zn_2SnO_4 and ZnO/Zn_2SnO_4, SnO_2/Zn_2SnO_4 layered-type sensors", *Sens. Actuators B*, vol. 72, pp. 141-148, 2001.

[23] S. Park, A. An, H. Ko, C. Jin, C. Lee, "Enhanced NO_2 sensing properties of Zn_2SnO_4 – core/ZnO-shell nanorod sensors", *Ceram. Int*. vol. 39, pp. 3539-3545, 2013

[24] V. V. Ganbavle, M. A. Patil, H. P. Deshmukh, K. Y. Rajpure, "Development of Zn_2SnO_4 thin films deposited by spray pyrolysis method and their utility for NO_2 gas sensors at moderate operating temperature", *J. Anal. Appl. Pyrol.*, vol. 107, pp. 233-241, 2014

[25] I. Stambolova, K. Konstantinova, D. Kovacheva, P. Peshev, T. Donchev, "Spray pyrolysis preparation and humidity sensing characteristics of spinel zinc-stannate thin films", *J. Solid State Chem.* Vol. 128, pp. 305-309, 1997

[26] D. Kovacheva, T. Bacalova, A. Batchvarov, K. Petrov, "Structural and humidity sensing characteristics of $Zn_{2-x}Mg_xSnO_4$ spinels" J. Mater. Sci. Lett. Vol. 20, pp. 1597-1599, 2001

[27] S. Zhang, G. Sun, Y. Li, B. Zhang, Y. Wang, Z. Zhang, "Enhanced triethylamine gas sensing performance of the porous Zn_2SnO_4/SnO_2 hiererachical microspheres", *J. Alloys Comp.*, vol. 785, pp. 382-390, 2019.

[28] J. Yang, S. Wang, L. Zhang, R. Dong, Z. Zhu, X. Gao, "Zn_2SnO_4-doped SnO_2 hollow spheres for phenylamine gas sensor application", *Sens. Actuators B Chem.* vol. 239, pp. 857-864, 2017.

[29] T. Islam, Md. R. Mahboob, S.A. Khan, "A simple MOX vapor sensor on polyimide substrate for measuring humidity in ppm level", *IEEE Sensors J.*, vol. 15, pp. 3004-3013, 2015.

[30] M. Rieu, M. Camara, G. Tournier, J.-P. Viricelle, C. Pijolat, N. F. de Rooij, D. Briand, "Fully inkjet printed SnO_2 gas sensor on plastic substrate", *Sens. Actuators B:Chem.*, vol. 236, pp. 1091-1097, 2016

[31] L. Manjakkal, B. Sakthivel, N. Gopalakrishnan, R. Dahiya, "Printed flexible electrochemical pH sensors based on CuO nanorods", *Sens. Actuators B: Chem.*, vol. 263, pp. 50-58, 2018.

[32] B. Sakhtivel, L. Manjakkal, G. Nammalvar, "High performance CuO nanorectangles based room temperature flexible NH_3 sensor", *IEEE Sensors J.*, vol. 17. pp. 6529-6536, 2017.

[33] A. Stein, S. W. Keller, T. E. Mallouk, Turning down the heat: design and mechanism in solid-state synthesis", *Science*, vol. 259, pp. 1558-1564, 1993.

[34] S. Ito, P. Chen, P. Comte, M. K. Nazeruddin, P. Liska, P. Pechy, M. Graetzel, "Fabrication of screen-printing pastes from TiO_2 powders for dye-sensitized solar cells", *Prog. Photovolt. Res. Appl.* vol. 15, pp. 603-612, 2007.

[35] M. V. Nikolic, Z. Z. Vasiljevic, M. D. Lukovic, V. P. Pavlovic, J. Vujancevic, M. Radovanovic, J. B. Krstic, B. Vlahovic, V. B. Pavlovic, "Humidity sensing properties of nanocrystalline pseudobrookite (Fe_2TiO_5) based thick films, *Sens. Actuators B. Chem.* vol. 277, pp. 654-664, 2018.

[36] Q. Ma, S. Wu, Y. Fan, "Synthesis and microwave dielectric properties of Zn_2SnO_4 ceramics", *Ceram. Int.*, vol. 40, pp. 1073-1080, 2014.

[37] E. Traversa, "Ceramic sensors for humidity detection: the state-of-the-art and future developments, *Sens. Actuators B*, vol. 23, pp. 135-156, 1995

[38] T. Lopes, L. Andrade, F. Le Formel, M. Gratzel, K. Sivula, A. Mendes, "Hematite photoelectrodes for water splitting: evaluation of the role of film thickness by impedance spectroscopy", *Phys. Chem. Chem. Phys*. Vol. 16, pp. 16515, 2014

[39] A. A. Saif, P. Poopalan, "Effect of the film thickness on the impedance behavior of sol-gel $Ba_{0.6}Sr_{0.4}TiO_3$ thin films", Physica B: Condens. Matter, vo. 406, pp. 1283-1288, 2011

[40] M. V. Nikolic, D. L. Sekulic, Z. Z. Vasiljevic, M. D. Lukovic, V. B. Pavlovic, O. S. Aleksic, "Dielectric properties, complex impedance and electrical conductivity of Fe_2TiO_5 nanopowder compacts and bulk samples at elevated temperatures", *J. Mater. Sci.:Mater. Electron*. vol. 28, pp. 4796-4806, 2017

[41] M. V. Nikolic, M. D. Lukovic, N. J. Labus, "Influence of humidity on complex impedance and dielectric properties of iron manganite ($FeMnO_3$)", *J. Mater. Sci.:Mater. Electron*. vol. 30, pp. 12399-12405, 2019

[42] N. Ponpandian, P. Balaya, A. Narayanasamy, "Electrical conductivity and dielectric behavior of nanocrystalline $NiFe_2O_4$ spinel", J. mPhys.:Condens. Matter vol. 14, pp. 3221-3236, 2002

[43] M. Slankamenac, T. Ivetic, M. V. Nikolic, N. Ivetic, M. Zivanov, V. B. Pavlovic, "Impedance response and dielectric relaxation in liquid-phase

sintered Zn_2SnO_4-SnO_2 ceramics, *J. Electron. Mater.* vol. 39, pp. 447-455, 2010.
[44] A. S. Bondarenko, G. Ragoisha, EIS Spectrum Analyzer http://www.abc.chemistry.bsu.by

Maria V. Nikolic (SM'2019) graduated at the Faculty of Electrical Engineering, University of Belgrade in 1990. She received a M.Sc. degree in electrical engineering in architecture and organization of computer networks in 1996 at the Faculty of Electronic Engineering, University of Belgrade. She obtained a Ph.D. degree in 2003 in materials science at the University of Belgrade. She is currently a Research Professor at the Institute for Multidisciplinary Research, University of Belgrade. Her current research interests include synthesis and characterization of oxide nanomaterials for humidity and gas sensors, thick film thermistors, sensors and devices based on them, photoelectrochemical cells, photocatalysts, ceramic and magnetic materials, sintering kinetics.

Milena P. Dojcinovic received B.Sc. and Master degrees' in Physical Chemistry in 2017 and 2018 at the Faculty of Physical Chemistry, University of Belgrade and is currently pursuing a Ph.D. student at the same Faculty. Since October 2018 she has been employed at the Institute for Multidisciplinary Research, University of Belgrade as a research assistant. Her current interests include synthesis and characterization of oxide nanomaterials for photocatalys, gas sensors and photoelectrochemical water splitting.

Zorka Z. Vasiljevic (formerly Djuric) obtained B. Sc., masters' diploma and Ph.D. in 2010, 2011 and 2019 at the Faculty of Technology and Metallurgy, University of Belgrade. She is currently working as research assistant at the Institute of Technical Sciences of SASA Her current interests include nanotechnology, synthesis and characterization of oxide materials for photoelectrochemical cells, photocatalysts and gas sensors, semiconductors and sintering.

Miloljub D. Lukovic was born on October 30, 1961. He received the B.S., M.S., and Ph.D. degrees in electrical engineering, all from University of Belgrade, Serbia, in 1988, 1993, and 2001 respectively. He is currently a research professor at the Institute for Multidisciplinary Research, University of Belgrade. His current research interests include experimental characterization of integrated thick-film LCV cells, thick film thermistors, sensors and devices based on them and EMI suppressors.

Nebojsa J. Labus obtained his B.Sc in 1999 at the Faculty of Physical Chemistry, University of Belgrade, M.Sc. degree in 2005 at the Technical Faculty, University of Kragujevac, and Ph.D. degree in 2011 at the Faculty of Physical Chemistry, University of Belgrade. Since 2001 he has been employed at the Institute of Technical Sciences of SASA, Belgrade, where he is now a Senior Research Associate. His research interest is mechanochemical activation, sintering and dilatometry.